IRBM 46 (2025) 100897

Contents lists available at ScienceDirect

IRBM

journal homepage: www.elsevier.com/locate/irbm

Elsevier Masson France
EM|consulte
www.em-consulte.com

Original Article

Hydrodynamic Alterations Produced by Subaortic Membranes: An *in Vitro* Study

Sofia Di Leonardo [a,b,1], Danila Vella [a,1], Calogera Pisano [c], Vincenzo Argano [c], Gaetano Burriesci [b,d,*,2]

[a] *Ri.MED Foundation, Palermo, Italy*
[b] *Department of Engineering, University of Palermo, Palermo, Italy*
[c] *Cardiac Surgery Unit, Policlinico Paolo Giaccone, University of Palermo, Palermo, Italy*
[d] *UCL Mechanical Engineering, University College London, London, UK*

HIGHLIGHTS

- Subaortic stenosis can significantly worsen the performance of the aortic valve.
- Membrane thickness and orifice size are crucial factors in disease severity.
- Membrane can increase leaflet fluttering, potentially leading to blood damage.
- A critical membrane size was identified, above which the impact becomes significant.
- In-vitro studies can help understand the complex effects of subaortic stenosis.

GRAPHICAL ABSTRACT

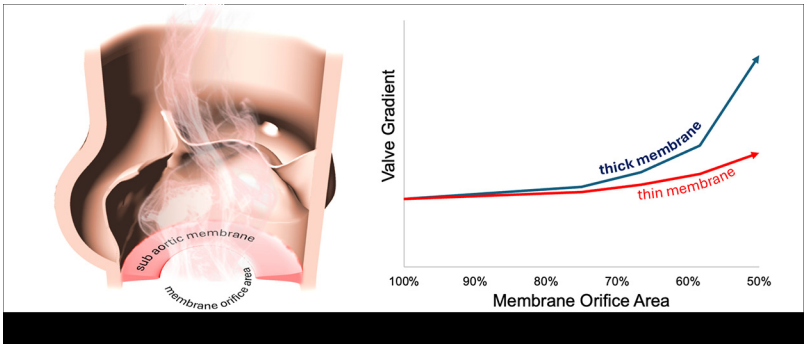

ARTICLE INFO

Article history:
Received 22 November 2024
Received in revised form 13 May 2025
Accepted 23 May 2025
Available online 28 May 2025

Keywords:
Subaortic stenosis
Subaortic membrane
In vitro analysis
Hydrodynamic performance
Leaflet fluttering

ABSTRACT

Background: Subaortic stenosis is an aortic disease characterised by the presence of a membrane located at the aortic valve inlet, that causes a sudden reduction of the inflow lumen. The membrane develops as a tissue growth of variable thickness that can cause a major increase in the pressure gradient. In this case, when diagnosed, it is removed by surgical resection.
Methods: To investigate the haemodynamic alteration introduced by subaortic membranes, an *in vitro* study was designed and performed. Stiff and flexible membranes were implanted at the inlet of a bioprosthetic control valve. These mock membranes had different radial and angular alignment, modelling concentric and eccentric orifice positions. For each configuration, a range of different membrane extensions was studied, progressively reducing the orifice area at the inlet of the control valve.
Results: Analysis of the hydrodynamic performances indicates that the detrimental effect of subaortic membranes becomes significant when the membrane orifice areas reduce below 75% of the unobstructed inflow lumen. Video analysis of the valve leaflets dynamics indicates that, together with a worsening in the systolic pressure gradient, the presence of subaortic membranes increases cusps fluttering. As the membrane orifice area reduces, leaflets experience faster oscillation frequencies at decreasing amplitudes.
Conclusions: The fibromuscular or thin nature of the membrane has a significant role on the severity of the pathology, with higher stiffnesses generally producing worse hydrodynamics. The orifice dimension

* Corresponding author at: University of Palermo, Department of Engineering, Palermo, Italy.
E-mail address: gaetano.burriesci@unipa.it (G. Burriesci).
[1] The first two authors contributed equally to this work.
[2] Postal address: University of Palermo, Department of Engineering, Viale delle Scienze, Ed. 8, 90128 Palermo, Italy.

https://doi.org/10.1016/j.irbm.2025.100897

and position are also important on the systolic performance and can determine potential structural degradation and haematic damage.

1. Introduction

Subaortic stenosis represents about 6.5% of adults' congenital heart disease [1]. Although it can be associated with several types of anatomic lesions, it is most commonly caused by the presence of a membrane positioned at the inflow of the aortic valve (in the 75-85% of the all cases [2]). This subaortic membrane (*SAM*) can assume the form of a discrete thin layer or of a thick fibromuscular ridge. *SAM* often occurs in the first decade of life, but it usually remains undiagnosed due to the absence of symptoms. When symptomatic, *SAM* is commonly diagnosed by 2D Doppler echocardiography examination of the flow within the left ventricular outflow tract (*LVOT*) [3]. If untreated, it can cause increased *LVOT* pressure gradient, left ventricular disfunction, and aortic regurgitation, becoming life trethening [4]. In these cases, the therapy consists in surgical resection of the membrane, that is associated to a high rate of pathology recurrence (18%) [5] and mortality of 3% [6]. The timing of intervention remains an open issue, with some groups advising to operate immediately to avoid further pathology progression, and other suggesting intervention only when specific conditions occur [3]. ACC/AHA guidelines recommend surgical intervention when the instantaneous peak of gradient of the *LVOT* echocardiographic Doppler exceeds 50 mmHg or the mean gradient is above 30 mmHg [7]. Regarding pathogenesis, there are two main hypotheses, the first one classifies *SAM* as a congenital disorder caused by genetic factors [8], the second identifies some haemodynamic factors as trigger of the pathology. This second hypothesis is supported by the established association of *SAM* with the presence of left ventricle abnormalities, which cause unphysiological blood flow [9,10]. Echocardiography has been widely used to evaluate the preoperative conditions of *SAM* patients, which are typically characterised by high mean and peak *LVOT* gradients, marked subaortic acceleration, and transition to turbulence [6,11]. Computational fluid dynamics studies have also been attempted to evaluate the role of haemodynamic factors in *SAM* [3,12]. However, the haemodynamics alteration introduced by *SAM* and their implications remain poorly understood. In particular, it is still unclear the effect of *SAM* type, shape and position on the aortic valve efficiency and the role of *SAM* on the leaflet fluttering and blood damage potential.

In this context, our study aims to investigate the haemodynamics associated with *SAM* by means of *in vitro* tests. In particular, the alterations in the fluid dynamic behaviour of a bioprosthetic aortic valve, introduced by the presence of different SAM configurations were assessed and compared, aiming to clarify the main pathological haemodynamic mechanisms affecting patients.

2. Methods

2.1. Test cases

A Carpentier-Edwards PERIMOUNT Magna Ease aortic valve (Edwards Lifesciences Corp, Irvine, CA, USA) of size 27 mm was selected as control case for this study. The valve was used to represent healthy valve performance, and then tested with different *SAM* conditions, simulated by introducing under the valve a subaortic membrane.

To simulate the cases of thick fibromuscular ridge *SAM* and discrete thin layer *SAM*, membranes were obtained from a sheet of ethylene-vinyl acetate foam 180 µm thick and with a Young's modulus of approximately 4 N/mm^2, and from a nitrile rubber 80 µm thick and with a Young's modulus of approximately 5 N/mm^2 (evaluated from standard uniaxial tests) [13], respectively. The two solutions offer very different flexural resistance, with the membranes obtained from the nitrile rubber sheet being more representative of the discrete thin SAM layer (called flexible), and the membranes obtained from the ethylene-vinyl acetate foam reproducing a behaviour closer to thick fibromuscular ridge *SAM* (called stiff).

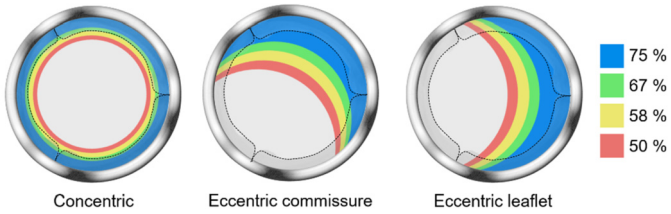

Fig. 1. The different shapes and setting of the subaortic membrane experimentally reproduced in the study.

To simulate different grades of obstruction, the membranes were laser cut to present, in the unloaded configuration, membrane orifice of areas (*MOA*) equal to 75%, 67%, 58% and 50% of the stent orifice area. To analyse the main *SAM* configurations observed clinically [14–16], membranes were cut as circular holes and positioned concentric to the valve (*Concentric* configuration), or obtained from the intersection of the stent orifice area with an identical profile, positioned eccentrically. For this case, the configuration with the orifice centre of area at a minimum distance from one of the leaflets base (*Eccentric leaflet* configuration) and from one of the valve commissures (*Eccentric commissure* configuration) were considered. Membranes were positioned 8 mm below the leaflet base, in compliance with the usual mean distance [17].

All analysed configurations are described in Fig. 1.

2.2. Hydrodynamic tests

In vitro tests were performed to evaluate the hydrodynamic function of the Perimount Magna Ease with and without the subaortic membrane. For this purpose, a ViVitro Pulse Duplicator system (ViVitro Labs, Victoria, Canada) was used, mounting in mitral position a Regent mechanical mitral valve (Abbott Cardiovascular, Plymouth, MN, USA) of size 29 mm. The system is equipped with Mikro-Cath pressure catheters (Millar, Houston, TX, USA), that record pressure in the atrial, ventricular and aortic chambers. As illustrated in Fig. 2, an electromagnetic flow probe with circular lumen of 28 mm diameter (Carolina Medical Electronics, East Bend, NC, USA) is positioned 35 mm below the membrane. A smooth, tapered section, positioned at the membrane inlet, gradually narrows the LVOT diameter from 28 mm to 24.6 mm, which corresponds to the inner valve diameter. The aortic chamber at the outflow of the valve includes a mock glass root with Valsalva sinuses and replicates physiological aortic compliance by Windkessel effect. In compliance with the standard ISO584 [18], tests were conducted at normal heartbeat of 70 bpm (cardiac cycle lasting 857 ms), with systole occupying 35% of the whole cycle. Each setup was tested at six cardiac outputs (CO) of 2, 3, 4, 5, 6, 7 l/min, applying a normotensive mean aortic pressure of 100 mmHg. The test fluid was phosphate-buffered saline solution at room temperature

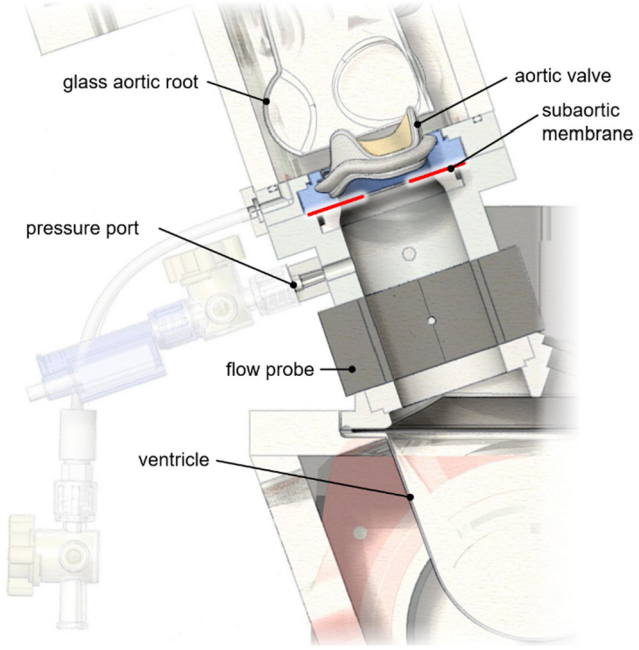

Fig. 2. Sketch of the experimental setup.

(Reynolds' number in the range 15,000-50,000, depending on the CO). This test fluid was selected to ensure consistency and reliability throughout the testing process, as substances commonly added to better replicate the physical properties of blood (e.g., glycerol) can adversely affect the mechanical response of valve tissue upon exposure [19].

For each test, the chambers pressures and the aortic flow curves were recorded for ten consecutive cycles, and used to calculate the hydrodynamic performance. In particular, systolic performance were assessed from the pressure gradient (ΔP) and the effective orifice area (EOA). ΔP is calculated as the mean value of the pressure difference across the aortic valve during positive systolic differential pressure period, and the EOA, representative of the *vena contracta* cross section at the aortic valve outflow, is estimated in square centimetres from the Gorlin's formula [20]:

$$EOA = \frac{q_{vRMS}}{51.6\sqrt{\frac{\Delta P}{\rho}}} \tag{1}$$

where ΔP is expressed in millimetres of mercury, q_{vRMS} is the root mean square forward flow during the positive differential pressure period, expressed in millilitres per second, and ρ is the density of the test fluid, expressed in grams per cubic centimetre.

Native and bioprosthetic valves are typically characterised by complete coaptation and negligible leakage when the valve is fully closed. Hence, diastolic performance were assessed in terms of closing regurgitant volume (*CRV*), corresponding to the regurgitant volume associated with the dynamics of the valve closure during a single cycle. This was estimated as the integral of the flow curve during the valve closing period.

The ventricular energy loss was taken as an indicator of the global valve performance, evaluated as sum of forward and closing energy loss ($E_{lossF} + E_{lossC}$), obtained from equation:

$$E_{loss} = 0.1333 \int_{t_s}^{t_f} \Delta p \cdot q_v(t) dt \tag{2}$$

where t_s and t_f are the start and finish instants of each phase, Δp and q_v are the instantaneous pressure drop and flow rate, expressed in millimetres of mercury and millilitres per second, respectively.

2.3. High frame rate video analysis

For each configuration, high frame rate (HFR) videos of five consecutive cardiac cycles were recorded from the valve outflow at a standard CO of 5 l/min, to observe the valve dynamics in the different scenarios. The videos were recorded with a HFR of 250 fps, using a led external light and a Sony RX0 II camera set on the top of the aortic chamber, perpendicular to the valve orifice. These were used to determine the projected dynamic valve area (*PDVA*) [21–23], defined as the instantaneous planimetric projection of the area encompassed within the valve leaflets on a plane orthogonal to the valve axis. This is commonly used as an estimate of the geometric orifice area (*GOA*) [24], although it strictly corresponds to the envelope of the *GOA* at the different cross sections within the valve area.

PDVA curves were analysed to estimate the frequency and amplitude of fluctuations, which are indicators of abnormal leaflet fluttering. In fact, the phenomenon has been associated with valve regurgitation, calcification and fatigue [21,24,25].

To analyse the HFR videos, a code was specifically written in Matlab (MathWorks, USA). Videos frames were processed by extracting the instantaneous planimetric projection area encompassed by the leaflets, by means of region growing technique. The resulting curves of the projected area varying in time, obtained for five consecutive cycles, were mediated to obtain the *PDVA* curves. The process is summarised in Fig. 2.

To evaluate leaflet fluttering, the systolic portion of each PDVA curve was identified as the region where the curve maintained non-zero values. To minimise the influence of valve opening and closing dynamics, the initial and final segments of this region were excluded, retaining only the central two-thirds of the systole for analysis. This selected segment of the PDVA curve was then decomposed into a sum of eight sinusoidal functions using the Curve Fitter Tool in MATLAB R2024a, employing a "Sum of Sine" regression model with eight terms. Among the resulting sinusoidal components, the one exhibiting the highest correlation with the PDVA peaks was selected as representative of the oscillation dominant frequency and amplitude (with reference to the right panel in Fig. 3, these correspond to $\omega/2\pi$ and $2a$, respectively).

3. Results and discussion

Fig. 4 summarises the hydrodynamic performance determined for each test. Expectedly, the control configuration with no membrane (black line) is associated with the best systolic performance, characterised by the lowest ΔP and the highest *EOA*. Stiff membranes, modelling the presence of a subaortic thick fibromuscular ridge, (top row) exhibit a progressive worsening in systolic performance with the reduction of the *MOA*. Looking at the different orifice shapes and positions, for the stiff membranes, concentric configurations (continuous lines) generally perform better than equivalent eccentric configurations at low COs. As the CO increases, eccentric configurations catch up, eventually becoming superior to the concentric at larger membrane orifices. The alignment of the orifice in the eccentric configurations does not produce relevant effect, with the leaflet alignment marginally superior for smaller membrane orifices and the commissural configuration becoming more favourable with smaller membrane sizes. Still, these differences are minor, and systolic performance for the thick membranes are well clustered based on the membrane orifice size, independently of the configurations.

In the case of flexible membranes, at low COs the worsening in systolic performance with the reduction of the *MOA* is very similar

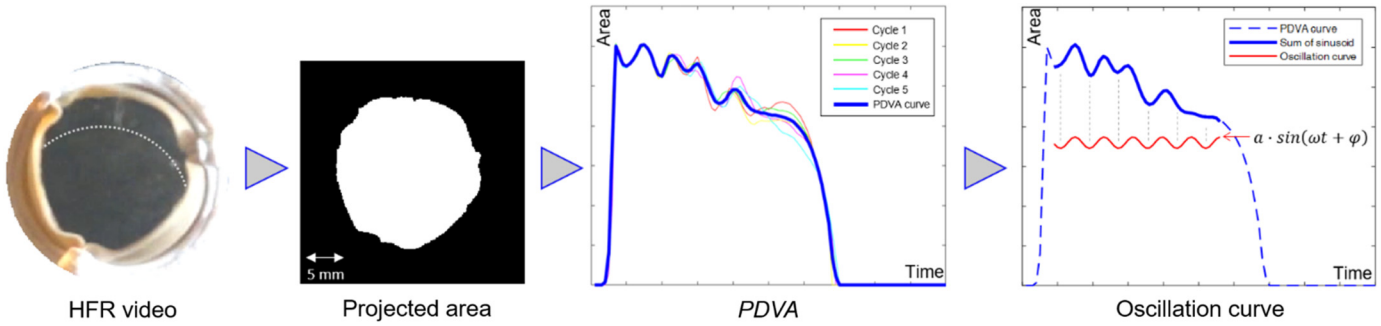

Fig. 3. Schematic sequence of operation performed to obtain PDVA curves and frequency and amplitude of leaflet fluttering.

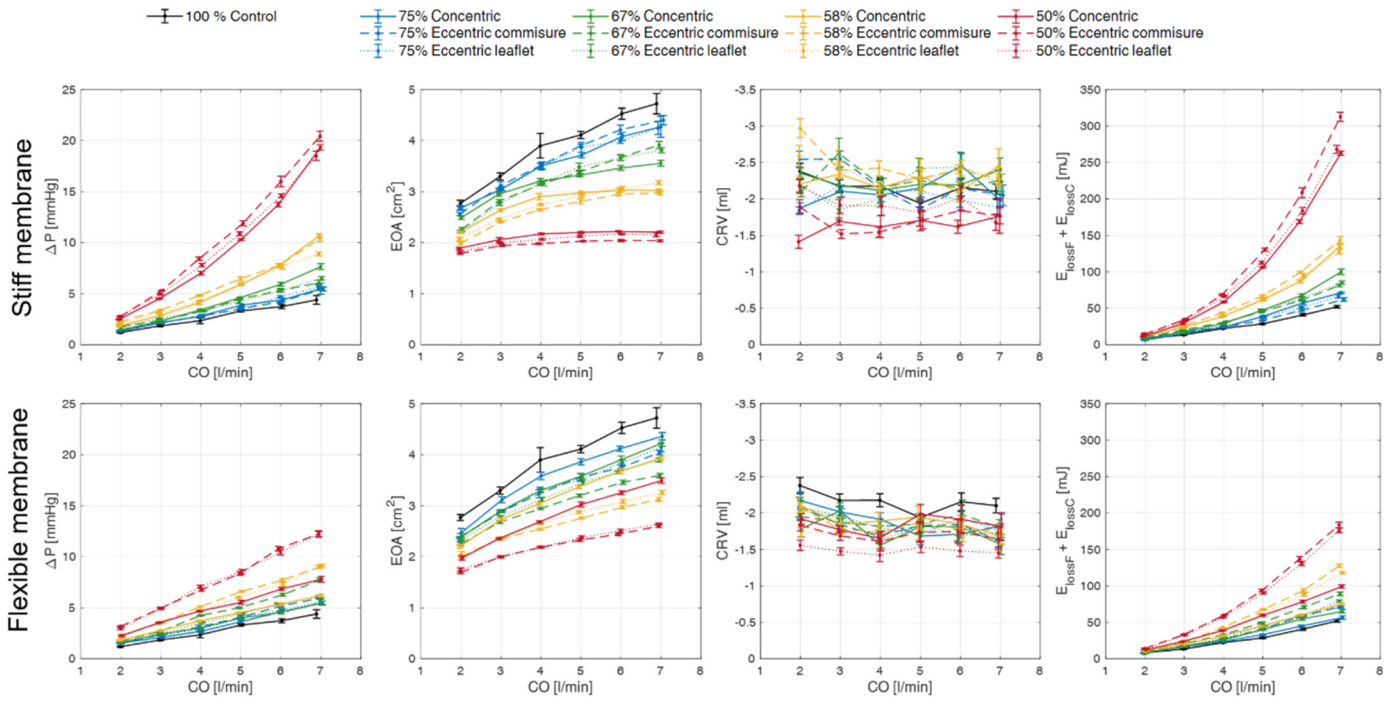

Fig. 4. From the left: ΔP, EOA, CRV and Energy loss are reported for all the test cases, where error bars represent the standard deviation.

to that observed for stiff membranes. However, it is substantially less severe as the CO increases. This is probably due to the ability of the membrane to deform under the effect of the larger transmembranal pressures generated by faster ejection flows. However, the improvement in systolic performance over stiff membranes is far more marked for concentric configurations, where the entire membrane orifice edge is free to deform. For eccentric configurations, where part of the membrane orifice is defined by the *LVOT* wall, and therefore remains identical for the stiff and flexible cases, the differences are reduced. The leaflet alignment is marginal but consistently favourable compared to the commissural alignment.

In terms of closing performance, stiff membranes present similar *CRV* values for all configurations, although the regurgitant volume with the smallest membrane orifice appears lower. This behaviour could be associated with the smaller *EOA*, that reduces the liquid volume encompassed by the open leaflets, which returns to the ventricle during coaptation. Moreover, smaller membrane orifices may result in some obstructive behaviour also for the backflow. These effects can be observed also for the flexible membranes, where the progressive reduction of *CRV* with the orifice is more apparent.

In general, the effect of the membrane size on the *CRV* is less obvious than the reduction in systolic performance, and has a marginal contribution to the overall efficiency. As a result, the global performance quantified through the energy losses shows similar trend to the *EOA* and ΔP curves sequence.

Fig. 5 summarises the variations introduced by the *SAM* on the hydrodynamic performance at a standard physiological CO of 5 l/min, as the *MOA* reduces. The effect of the membrane on the ΔP starts becoming relevant when the *MOA* reduces below 75%. In particular, in the case of the stiff membrane, eccentric configurations have a negligible effect up to this membrane dimension, while the central orifice results in slightly larger ΔP and smaller *EOA*. As the *MOA* reduces further, the concentric configuration becomes somewhat more advantageous, although all curves remain well clustered. In the case of flexible membranes, on the contrary, the concentric configuration results significantly superior for all membrane dimensions, and becomes substantially more efficient than all other configurations at small *MOA*s. Flexible membrane eccentric configurations appear inferior to stiff membrane configurations for medium-large orifices, becoming better performing when the *MOA* reduces below 60%. In general, their overall efficiency is comparable to that of stiff membrane configurations.

In terms of *CRV*, flexible membranes are consistently better than stiff membranes. However, as mentioned above, the contribution of this component to the overall valve performance is small compared to the systolic parameters, so it does not significantly affect the total energy loss.

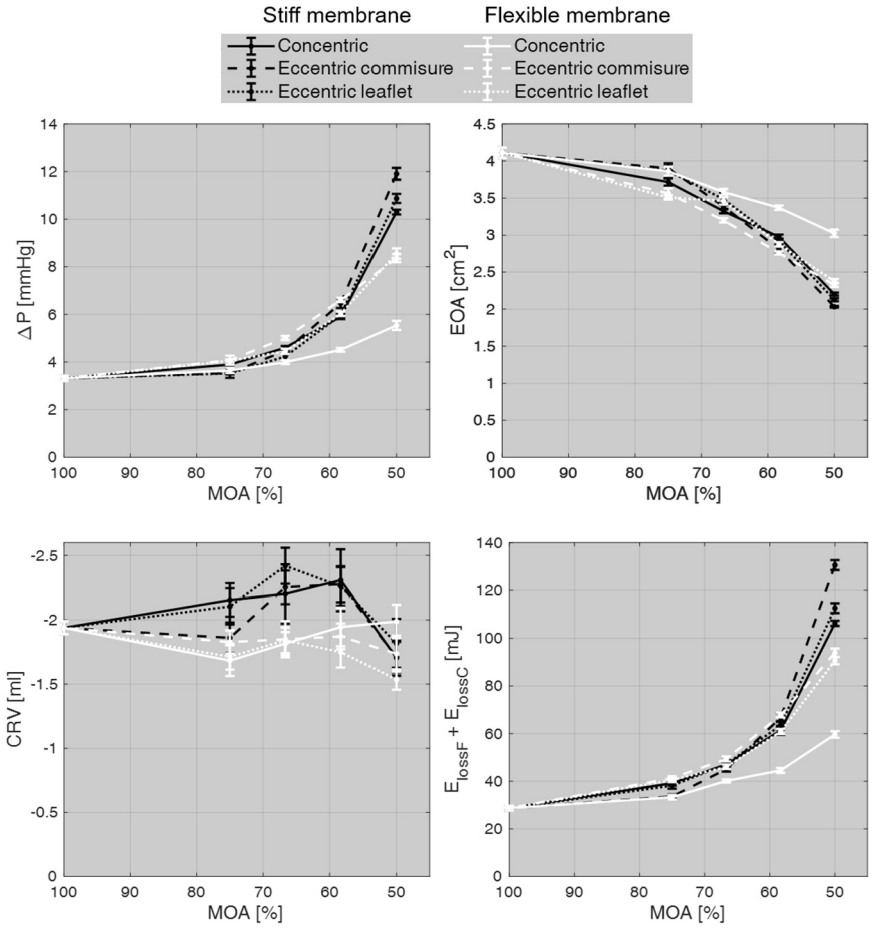

Fig. 5. ΔP, EOA, CRV and Energy loss performance at CO 5 l/min, where error bars represent the standard deviation.

Fig. 6 reports the *PDVA* for the different *MOA*s, averaged over five cardiac cycles at a CO of 5 l/min and normalised over the internal stent cross section. In the same figure, a bar chart of the fluttering frequencies and amplitudes estimated for the different *MOA*s is represented. As mentioned above, the analysis of fluttering is particularly interesting, as the phenomenon has been associated with early leaflet calcification, blood damage and fatigue failure [25–27].

All *PDVA* curves are characterised by an initial peak of similar value, followed by a reduction in the projected area at decreasing *MOA*. Hence, after the peak, one or more leaflets may move to an intermediate semi-open configuration, depending on the size and alignment of the membrane orifice. Still, it is essential to observe that for all cases the valve experiences a full opening at the early systole, thus reducing the consequences of the loss of motility, which may otherwise induce remodelling of fibrous connective tissue and commissural fusion [28]. This leaflet opening mechanism has also been reported in other clinical studies, where increased leaflet fluttering associated with a subaortic membrane is attributed to a focused jet created by the membrane, which impinges directly on the leaflets [12].

Frequency of the control valve resulted equal to 24.41 Hz, which is consistent with the cycle of vibration determined by Lee et al. 2021 (26.03 Hz) for a pericardial bioprosthetic valve of equivalent diameter [21].

In general, the *PDVA* analysis supports the findings from the hydrodynamics assessment, confirming that the stiff membrane produces larger changes than the flexible membrane. In particular, the presence of the stiff membrane causes a rapid *PDVA* reduction in the first milliseconds after the initial peak, reduction that starts earlier and becomes steeper as the *MOA* decreases (from 75% to 50%). This jump is absent in the control case and in all flexible membrane configurations.

MOA reductions are also associated with increase in fluttering. In the case of stiff membranes, the oscillation frequencies increase of over two folds within the analysed range. Expectedly, the maximum frequency for the concentric and eccentric commissure configurations is achieved for the smallest *MOA* of 50% (reaching 51 Hz and 58 Hz, respectively). Interestingly, for the eccentric leaflet configuration, minimum fluttering amplitude is observed for an intermediate *MOA* of 67%. This is associated with a maximum oscillation frequency (51 Hz), although the *PDVA* is very smooth. For further reductions in the membrane orifice, a progressive increase in amplitude is observed, associated with a reduction in fluttering frequency. This is due to the fact that, as the *MOA* reduces below 67%, the membrane focuses the systolic jet on a single leaflet, leaving the other two in a semi-open configuration.

In the case of flexible membranes, fluttering frequencies are generally slower than with stiff membranes at similar amplitudes. The oscillatory behaviour of eccentric configurations is less dependent on the *MOA*, except for the smallest orifice in the eccentric leaflet configuration, which is characterised by very little oscillations at higher frequencies. As for the stiff membrane, one of the eccentric leaflet configurations produces a smooth *PDVA*, characterised by minimum fluttering at high frequencies (43 Hz). However, this is achieved for the smallest *MOA* of 50%.

The findings were obtained using a PBS solution, which may introduce some systematic differences in the hydrodynamic performance. However, employing a blood-equivalent fluid could ad-

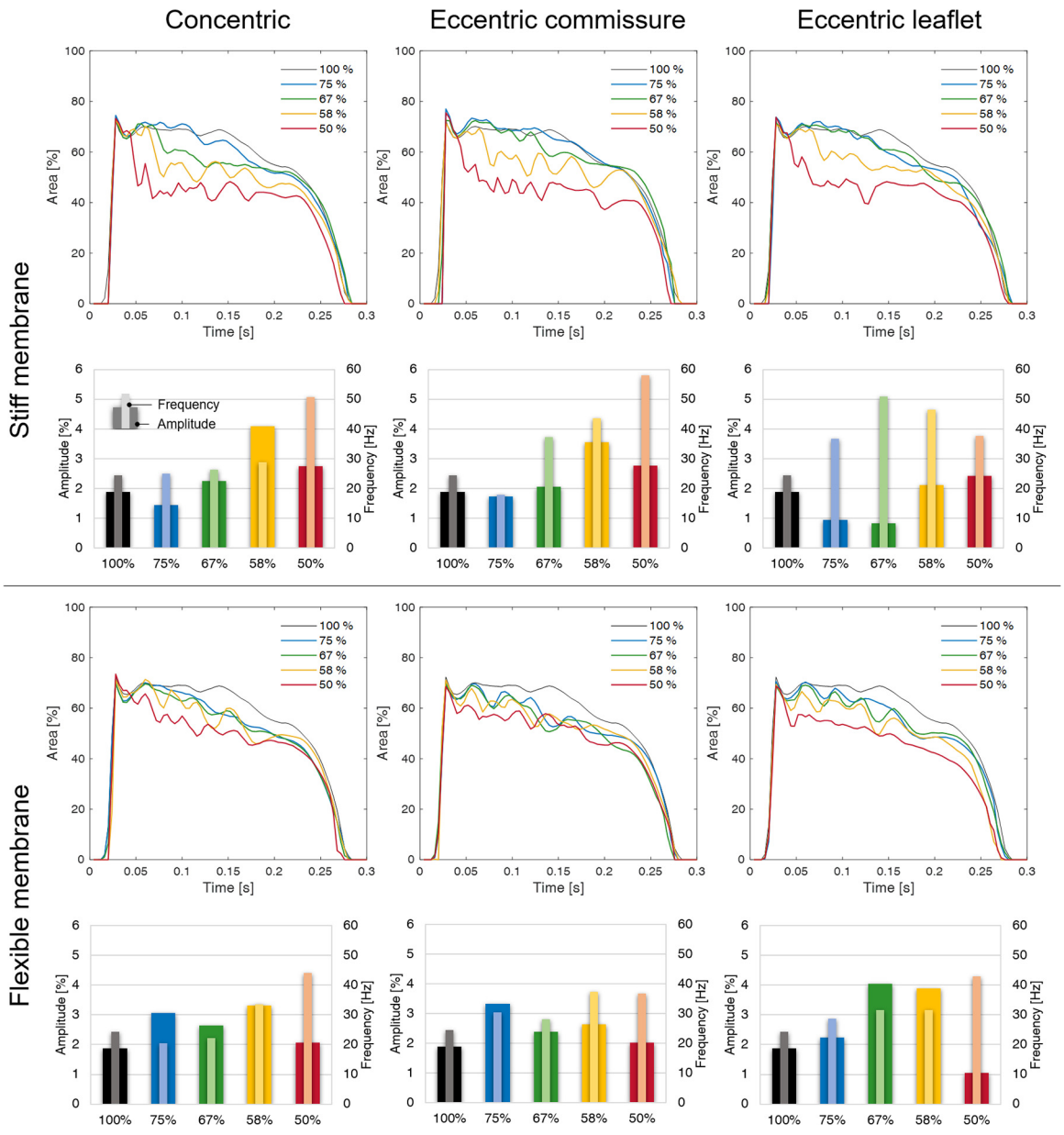

Fig. 6. Top: mean PDVA instantaneous value over five cardiac cycles at CO5 l/min. Bottom: frequency (thin bar) and amplitude (thick bar) of the leaflet fluttering computed from the PDVA curve for each studied case. The percentages indicate the area of the outflow free from the obstruction.

versely affect the consistency and reliability of the results, by causing progressive leaflet stiffening across the testing process [19].

In general, it is interesting to observe some correspondence in the trend determined for the fluttering oscillation and the *CRV*. An association between fluttering and valve regurgitation has already been suggested in the literature [25], although the mechanism for the phenomenon is not described. Our study suggests that large oscillation may be an index/cause of higher turbulence, which can perturb the physiological vortical structures that, in healthy conditions, facilitate a prompt closing [29,30]; hence cause increased *CRV*. As mentioned above, the contribution of this loss to the overall efficiency is normally negligible, but the implications in terms of blood damage from shear-induced thrombocyte activation may be of some concern [26].

The findings of this study have important clinical implications for the management of patients affected by SAM. Specifically, the presented results suggest that surgical decision should not rely solely on the mean gradient, but must also consider the membrane orifice area and morphology. Patients presenting with an eccentric subcommissural fibromuscular SAM appear to be at higher risk and should be treated at an earlier stage to prevent aortic valve degeneration and more complex delayed surgical procedures. A comprehensive assessment of the membrane characteristics may guide timely surgical interventions and improve patient outcomes.

4. Conclusion

This work analyses the haemodynamic alteration introduced by *SAM*s. The disease was simulated by introducing flexible and stiff membranes under a Perimount control valve, designed to reproduce various degrees of obstruction with different radial and angular position. Results indicate that the hydrodynamic alterations at the aortic root are significantly influenced by a number of factors, including the fibromuscular of thin nature of the membrane, its extension and its shape. The *MOA* results the dominant parameter, with the systolic performance worsening as this decreases. In particular, the presence of the membrane is felt significantly only when the *MOA* reduces below 75%. For smaller orifices, the gradi-

ent of trans-LVOT pressure difference increases as the membrane extends. The effect is stronger for membranes with lower deformability, such as fibromuscular rims. An important role is also played by *MOA* position, especially in the case of thin membranes: concentric orifices present better performance compared with the eccentric positions, and orifices positioned below one of the leaflets are generally slightly more favourable that orifices positioned below commissures. The study has also shown that the presence of SAMs is associated with a substantial increase in fluttering of the aortic leaflets, whose oscillation frequency generally increases with *MOA* reduction. This is an indicator of the potential presence of turbulence, which can promote valve and aortic tissue degradation as well as blood damage. Moreover, the effect appears to be associated to some increase in valve regurgitation during closing. Finally, the study highlights the role of *in vitro* investigations in providing a controlled environment for studying pathological aspects that are difficult to isolate clinically, ultimately enhancing our understanding of complex physiological processes.

CRediT authorship contribution statement

Sofia Di Leonardo: Writing – original draft, Visualization, Validation, Software, Investigation, Formal analysis, Data curation, Conceptualization. **Danila Vella:** Writing – original draft, Visualization, Validation, Software, Investigation, Formal analysis, Data curation, Conceptualization. **Calogera Pisano:** Writing – original draft, Visualization, Validation, Investigation, Conceptualization. **Vincenzo Argano:** Writing – original draft, Visualization, Validation, Investigation, Conceptualization. **Gaetano Burriesci:** Writing – review & editing, Visualization, Validation, Supervision, Project administration, Methodology, Investigation, Conceptualization.

Author contributions

All authors attest that they meet the current International Committee of Medical Journal Editors (ICMJE) criteria for Authorship.

Funding

This work did not receive any grant from funding agencies in the public, commercial, or not-for-profit sectors.

Declaration of competing interest

The authors declare that they have no known competing financial or personal relationships that could be viewed as influencing the work reported in this paper.

References

[1] Aboulhosn J, Child JS. Left ventricular outflow obstruction. Circulation 2006;114:2412–22. https://doi.org/10.1161/CIRCULATIONAHA.105.592089.
[2] Perez Y, Dearani JA, Miranda WR, Stephens EH. Subaortic stenosis in adult patients with atrioventricular septal defect. Ann Thorac Surg 2023;115:479–84. https://doi.org/10.1016/j.athoracsur.2022.08.011.
[3] Massé DD, Shar JA, Brown KN, Keswani SG, Grande-Allen KJ, Sucosky P. Discrete subaortic stenosis: perspective roadmap to a complex disease. Front Cardiovasc Med 2018;5. https://doi.org/10.3389/fcvm.2018.00122.
[4] Devabhaktuni SR, Chakfeh E, Malik AO, Pengson JA, Rana J, Ahsan CH. Subvalvular aortic stenosis: a review of current literature. Clin Cardiol 2018;41:131–6. https://doi.org/10.1002/clc.22775.
[5] Bandara D, Salve GG, Marathe SP, Betts KS, Cole AD, Ayer JG, et al. Mid- and long-term outcomes after surgical correction of subaortic stenosis: a 27-year experience. Eur J Cardio-Thorac Surg 2023;64. https://doi.org/10.1093/ejcts/ezad314.
[6] van der Linde D, Roos-Hesselink JW, Rizopoulos D, Heuvelman HJ, Budts W, van Dijk APJ, et al. Surgical outcome of discrete subaortic stenosis in adults. Circulation 2013;127:1184–91. https://doi.org/10.1161/CIRCULATIONAHA.112.000883.
[7] Warnes CA, Williams RG, Bashore TM, Child JS, Connolly HM, Dearani JA, et al. ACC/AHA 2008 guidelines for the management of adults with congenital heart disease. J Am Coll Cardiol 2008;52:e143–263. https://doi.org/10.1016/j.jacc.2008.10.001.
[8] Fatimi SH, Ahmad U, Javed MA, Shamim S, Ahmad R. Familial membranous subaortic stenosis: review of familial inheritance patterns and a case report. J Thorac Cardiovasc Surg 2006;132:1484–14861.e. https://doi.org/10.1016/j.jtcvs.2006.08.034.
[9] Cape EG, VanAuker MD, Sigfússon G, Tacy TA, del Nido PJ. Potential role of mechanical stress in the etiology of pediatric heart disease: septal shear stress in subaortic stenosis. J Am Coll Cardiol 1997;30:247–54. https://doi.org/10.1016/S0735-1097(97)00048-X.
[10] Foker JE. Outcomes and questions about discrete subaortic stenosis. Circulation 2013;127:1447–50. https://doi.org/10.1161/CIRCULATIONAHA.113.001619.
[11] Pickard SS, Geva A, Gauvreau K, del Nido PJ, Geva T. Long-term outcomes and risk factors for aortic regurgitation after discrete subvalvular aortic stenosis resection in children. Heart 2015;101:1547–53. https://doi.org/10.1136/heartjnl-2015-307460.
[12] Davis RH, Feigenbaum H, Chang S, Konecke LL, Dillon JC. Echocardiographic manifestations of discrete subaortic stenosis. Am J Cardiol 1974;33:277–80. https://doi.org/10.1016/0002-9149(74)90289-6.
[13] International Standard. ISO 37:2011 Rubber, vulcanized or thermoplastic — Determination of tensile stress-strain properties. 2011.
[14] Ku L, Ma X. A subaortic membrane causing left ventricular outflow tract obstruction. Radiology 2024;310. https://doi.org/10.1148/radiol.232805.
[15] Hatab T, Zaid S, Toro S, Wessly P, Malahfji M, Faza N, et al. Now you see me now you don't: subaortic membrane causing a diagnostic dilemma. JACC Case Rep 2023;18. https://doi.org/10.1016/j.jaccas.2023.101916.
[16] Butany J, Ahluwalia MS, Fayet C, Munroe C, Blit P, Ahn C. Hufnagel valve: the first prosthetic mechanical valve. Cardiovasc Pathol 2002:11. https://doi.org/10.1016/S1054-8807(02)00132-1.
[17] Motro M, Schneeweiss A, Shem-Tov A, Benjamin P, Kaplinsky E, Hegesh J. Correlation of distance from subaortic membrane to base of the right aortic valve cusp and the development of aortic regurgitation in mild discrete subaortic stenosis. Am J Cardiol 1989;64:395–6. https://doi.org/10.1016/0002-9149(89)90544-4.
[18] ISO 5840-1:2021 (E) Cardiovascular Implants Cardiac Valve Prosthes — Part 1: General requirements. International Organization for Standardization, Geneva, Switzerland n.d.
[19] Parker R, Randev R, Wain WH, Ross DN. Storage of heart valve allografts in glycerol with subsequent antibiotic sterilisation. Thorax 1978;33. https://doi.org/10.1136/thx.33.5.638.
[20] Gorlin R, Gorlin SG. Hydraulic formula for calculation of the area of the stenotic mitral valve, other cardiac valves, and central circulatory shunts. I. Am Heart J 1951;41. https://doi.org/10.1016/0002-8703(51)90002-6.
[21] Lee JH, Scotten LN, Hunt R, Caranasos TG, Vavalle JP, Griffith BE. Bioprosthetic aortic valve diameter and thickness are directly related to leaflet fluttering: results from a combined experimental and computational modeling study. JTCVS Open 2021;6:60–81. https://doi.org/10.1016/j.xjon.2020.09.002.
[22] Di Leonardo S, Vella D, Grillo CS, Martorana C, Torre S, Argano V, et al. Hydrodynamic ex vivo analysis of valve-sparing techniques: assessment and comparison. Eur J Cardio-Thorac Surg 2023;63. https://doi.org/10.1093/ejcts/ezad040.
[23] Susin FM. Complete unsteady one-dimensional model of the net aortic pressure drop. Open Biomed Eng J 2019;13:83–93. https://doi.org/10.2174/1874120701913010083.
[24] Garcia D, Pibarot P, Landry C, Allard A, Chayer B, Dumesnil JG, et al. Estimation of aortic valve effective orifice area by Doppler echocardiography: effects of valve inflow shape and flow rate. J Am Soc Echocardiogr 2004;17:756–65. https://doi.org/10.1016/j.echo.2004.03.030.
[25] de Avelar AH F, Canestri JA, Bim C, Silva MGM, Huebner R, Pinotti M. Quantification and analysis of leaflet flutter on biological prosthetic cardiac valves. Artif Organs 2017;41:835–44. https://doi.org/10.1111/aor.12856.
[26] Johnson EL, Wu MCH, Xu F, Wiese NM, Rajanna MR, Herrema AJ, et al. Thinner biological tissues induce leaflet flutter in aortic heart valve replacements. Proc Natl Acad Sci 2020;117:19007–16. https://doi.org/10.1073/pnas.2002821117.
[27] Avelar AH de F, Stófel MAGE, Canestri JA, Huebner R. Analytical approach on leaflet flutter on biological prosthetic heart valves. J Braz Soc Mech Sci Eng 2017;39:4849–58. https://doi.org/10.1007/s40430-017-0908-4.
[28] Martina JR, Schipper MEI, de Jonge N, Ramjankhan F, de Weger RA, Lahpor JR, et al. Analysis of aortic valve commissural fusion after support with continuous-flow left ventricular assist device. Interact Cardiovasc Thorac Surg 2013;17:616–24. https://doi.org/10.1093/icvts/ivt263.
[29] Toninato R, Salmon J, Susin FM, Ducci A, Burriesci G. Physiological vortices in the sinuses of valsalva: an in vitro approach for bio-prosthetic valves. J Biomech 2016;49:2635–43. https://doi.org/10.1016/j.jbiomech.2016.05.027.
[30] Tango AM, Salmonsmith J, Ducci A, Burriesci G. Validation and extension of a fluid–structure interaction model of the healthy aortic valve. Cardiovasc Eng Technol 2018;9:739–51. https://doi.org/10.1007/s13239-018-00391-1.